time independent. Thermal expansion coefficients of the composites in three principal directions are $\alpha_{11} = -0.5 \times 10^{-6}/°C$ and $\alpha_{22} = \alpha_{33} = 40.0 \times 10^{-6}/°C$, where the negative value indicates shrinkage with temperature increase.

Figures 3 and 4 show radial displacement and radial stress profiles across the thickness of the cylinder at three instants, $t = 10^{-3}$ min, $t = 10^{4.5}$ min, and $t = 10^{12}$ min, respectively. The radial tractions and displacements satisfied the continuity conditions at the interfaces of layers at all instants. The saw-shaped radial stress distribution is resulted from the discontinuity of material properties and various fiber orientations. The radial displacement $w(t)$ reaches a steady state at $T = 10^{12}$ min due to a long-term creep behavior. The radial displacement of most layers reaches a constant value, except at the innermost and outermost portions of the cylinder. The free traction boundary at the surface of cylinders causes the gradients in the radial displacements. A similar phenomenon is also observed in the radial stresses showing a constant level of stress distribution in the inner portion of cylinder away from boundary layers at $t = 10^{12}$ min. This long-term creep characteristic reflects the proposed power law form, Eqs. (19) and (20), of the creep compliances.

IV. Conclusions

An analysis was developed to study the thermal viscoelastic behavior of thick-walled laminated composite cylinders. The formulation accounts for ply-by-ply variations of material properties and temperature changes. The matrix form numerical solution with parallel computing techniques resolved the complexity and time-consuming calculation procedures in the Laplace transform of a multilayered composite cylinder. The creep behavior of materials and relaxation of thermal stresses in a cylinder subjected to a uniform temperature change were properly predicted illustrating the capability of the analysis. Because the viscoelastic properties exist only in matrix dominant properties, such as transverse and shear properties, the viscoelastic behavior of anisotropic laminated cylinders is quite different from those of isotropic cylinders. The stresses will not diminish due to elastic properties in the fiber direction. The developed analysis will be very useful to study the viscoelastic behavior of cylinders under thermal loads and thermal residual stresses due to the manufacturing processes of thermoplastic composites.

References

[1]Biot, M. A., "Linear Thermodynamics and the Mechanics of Solids," *Proceedings, 3rd U.S. National Congress of Applied Mechanics*, American Society of Mechanical Engineers, New York, 1958, pp. 1–18.

[2]Muki, R., and Sternberg, E., "On Transient Thermal Stresses in Viscoelastic Materials with Temperature Dependent Properties," *Journal of Applied Mechanics*, Vol. 28, Series E, No. 2, 1961, pp. 193–207.

[3]Schapery, R. A., "Application of Thermodynamics to Thermomechanical, Fracture, and Birefringent Phenomena in Viscoelastic Media," *Journal of Applied Physics*, Vol. 35, No. 5, 1964, pp. 1451–1465.

[4]Williams, M. L., "Structural Analysis of Viscoelastic Materials," *AIAA Journal*, Vol. 2, No. 5, 1964, pp. 785–808.

[5]Christensen, R. M., *Theory of Viscoelasticity, An Introduction*, 2nd ed., Academic, New York, 1982.

[6]Hashin, Z., "Viscoelastic Behavior of Heterogeneous Media," *Journal of Applied Mechanics*, Vol. 32, Series E, No. 3, 1965, pp. 630–636.

[7]Schapery, R. A., "Stress Analysis of Viscoelastic Composite Materials," *Journal of Composite Materials*, Vol. 1, No. 3, 1967, pp. 228–267.

[8]Rogers, T. G., and Lee, E. H., "The Cylinder Problem in Viscoelastic Stress Analysis," *Quarterly of Applied Mathematics*, Vol. 22, No. 2, 1964, pp. 117–131.

[9]Tzeng, J. T., and Chien, L. S., "A Thermal/Mechanical Model of Axially Loaded Thick-Walled Composite Cylinders," *Journal of Composites Engineering*, Vol. 4, No. 2, 1994, pp. 219–232.

[10]Chien, L. S., and Tzeng, J. T., "A Thermal Viscoelastic Analysis for Thick-Walled Composite Cylinders," *Journal of Composite Materials*, Vol. 29, No. 4, 1995, pp. 525–548.

[11]Kim, R. Y., and Hartness, J. T., "Time-Dependent Response of AS-4/PEEK Composite," *Proceedings of the 19th International SAMPE Technical Conference*, Society for the Advancement of Material and Process Engineering, Covina, CA, 1987, pp. 468–475.

Correlation of Shock Angles Caused by Rhombic Delta Wings

S. Koide,*C. J. W. Griesel,† and J. L. Stollery‡
Cranfield University,
Bedford, England, United Kingdom

Introduction

In the past five years, the authors have investigated the effects of strakes on the glancing shock-wave/turbulent-boundary-layer interaction generated by an unswept sharp fin placed on a wall (see Fig. 1).[1,2] To consider the role of the shock structure on the interaction behavior, the inviscid flowfields around the fin with one of several different strakes were calculated by an Euler computational fluid dynamics (CFD) solver. Figure 1 shows a three-dimensional inviscid-shock structure deduced from the computed flowfields. The shock structure consists of two shock waves, one from the strake and the other from the unmodified part of the fin, and they are expressed by strake shock and fin shock, respectively, in Fig. 1. To consider the roles of the shocks, traces of the two shock waves on the wall provided important reference positions (the imaginary positions that would exist if no boundary layer were presented on the wall). But no simple solutions existed to predict these positions. In this Note, flowfields around a series of rhombic delta wings (RDWs; see Fig. 2) are calculated by the Euler CFD solver to predict the strake shock location on the wall. This is because the RDWs generate inviscid shock waves appropriate to the strake shock. Using the computed data, a correlation law with Mach number M and wing geometry is constructed for predicting the shock angle in the plane of symmetry of the wing β (see Fig. 2, corresponding to the strake-shock angle on the wall of Fig. 1). Once the shock angle is predicted using the correlation law, the strake-shock trace can be specified on the wall as long as the shock remains attached to the strake apex. As to the fin-shock location, a prediction method has been proposed in Refs. 1 and 2.

Computation Method

An Euler CFD code developed by Griesel[3] was employed for the present configurations. In Griesel's solver, a Riemann-problem-based, shock-capturing method was applied to the solution of the steady Euler equations. The code has already been well validated using two-dimensional models such as a wedge in a duct, a backward-facing ramp, and a biconvex airfoil.[3] In addition, the computed shock angles β for a rhombic delta wing (see Fig. 2) were compared with experimental angles obtained by schlieren photography. They were in excellent agreement for wing half-apex angles α ranging from 8 to 14 deg and for wing sweep angles λ of 45 and 60 deg at $M = 2.45$.[1]

Correlation of the Shock Angles

To collect data for constructing a correlation law of the shock angle β with M and the wing geometry (as specified by α and λ, see Fig. 2), flowfields around a series of RDWs were calculated by the Euler CFD solver. The CFD calculations were carried out for RDWs with $30 \leqq \lambda \leqq 60$ deg and $8 \leqq \alpha \leqq 17$ deg ($\leqq 14$ deg at $M = 2.0$) at $M = 2.0$, 2.46, and 3.5. This range was chosen to include the experimental condition of Refs. 1 and 2, together with a wider band of supersonic Mach numbers under which the shock wave remains attached to the delta wing apex. Figure 2 shows an example of the computed pressure field in the plane of symmetry. The solid circles

Received April 19, 1995; revision received Aug. 11, 1995; accepted for publication Aug. 11, 1995.

*Ph.D. Student, College of Aeronautics; currently Senior Research Engineer, 2-5th Lab., 3rd Research Centre, Japan Defense Agency, 1-2-10 Sakae, Tachikawa, Tokyo 190, Japan. Member AIAA.

†Ph.D. Student, College of Aeronautics. Student Member AIAA.

‡Professor, Head of College of Aeronautics. Fellow AIAA.

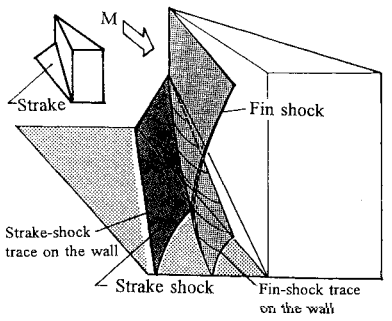

Fig. 1 Inviscid shock structure around a sharp fin with a strake.

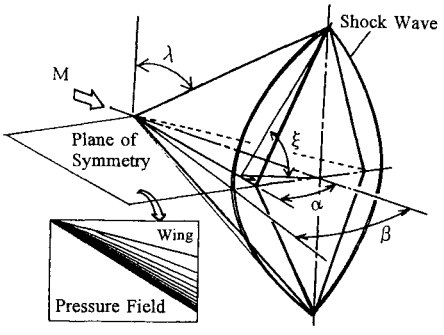

Fig. 2 Schematic view of a rhombic delta wing and its inviscid shock wave.

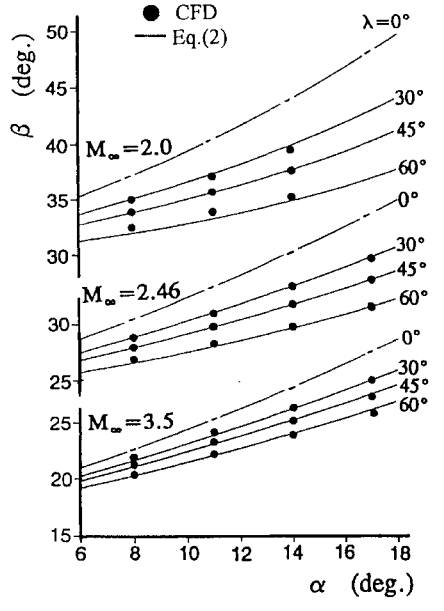

Fig. 3 Comparison of the shock wave angles obtained by the CFD procedures and Eq. (2).

in Fig. 3 are the values of β read from the pressure fields computed at $M = 2.0$, 2.46, and 3.5.

To predict the shock angle for arbitrary M, α, and λ, β must be correlated with them. To construct the correlation law, the angle between the plane of symmetry and the face of the delta wing,

$$\xi = \tan^{-1} \frac{1}{\sin \alpha \tan \lambda} \tag{1}$$

(see Fig. 2) was introduced. When α and λ increase, ξ tends to depart from 90 deg. Similarly β will decrease from its value at $\lambda = 0$ deg (i.e., the oblique shock angle for an unswept sharp fin of half-wedge angle α, expressed by β_{os}, see the case of $\lambda = 0$ deg in Fig. 3) as ξ drops below 90 deg. Hence, a simple correlation between ξ and

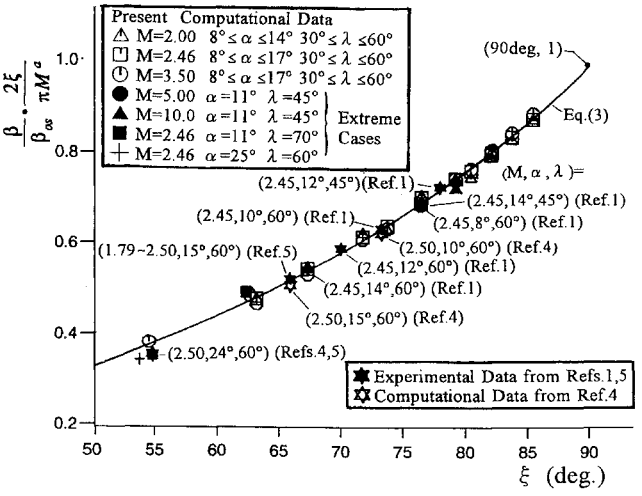

Fig. 4 Correlation of the shock angles.

β/β_{os} was first examined but did not sufficiently collapse the data obtained at different M.[1] To improve the correlation, the parameter

$$(\beta/\beta_{os}) \cdot (2\xi/\pi M^a)$$

has been finally developed, where ξ is expressed in radians and the power a has been selected as $(\pi/2 - \xi)/3$. From Fig. 3, it has been noticed that β drops less from β_{os} as M increases. As a result, β/β_{os} increased with M for a fixed ξ. This tendency was considered in the parameter using the variable M. In addition to the effect of M, it has been understood from the relationship linking β, β_{os}, and ξ that β has to approach β_{os} when ξ approaches 90 deg. To satisfy this condition, expressions of $\pi/2 - \xi$ and $2\xi/\pi$ (90 − ξ and ξ/90 in degrees) were employed. The number 3 of the power a was chosen purely for improving the correlation. Consequently, this parameter greatly improved the data correlation with ξ (see △, □, and ○ in Fig. 4).

The value of β is then determined directly from

$$\beta = \frac{\pi \beta_{os} F(\xi) M^a}{2\xi} \tag{2}$$

where $F(\xi)$ was obtained by the least-squares method as

$$F(\xi) = -0.2504 + 0.8081\xi - 0.1829\xi^2 - 0.0971\xi^3 + 0.1318\xi^4 \tag{3}$$

A fourth-order equation was necessary to correlate the data over a wide range of ξ. Each coefficient of Eq. (3) was adjusted for Eq. (3) to pass through the point (90 deg, 1) in Fig. 4. But a slight error from the point was inevitable because of the approximation using the least-squares method. (See the upper right corner of Fig. 4.) With Eq. (3) and the expressions of $\pi/2 - \xi$ (in the power a) and $\pi/(2\xi)$, Eq. (2) provides β of almost β_{os} when ξ is 90 deg. The values of β obtained by the CFD calculations and Eq. (2) are compared in Fig. 3 at various M, α, and λ. The agreement is very good.

To check the validity of this procedure, experimental and computational RDW shock angles obtained by Koide,[1] Deng et al.,[4] and Liao and Deng[5] are plotted by star-shaped symbols on Fig. 4. All of them are quite close to the correlation line. Additionally some extreme cases were calculated to estimate the effective range of Eq. (2) (see ●, ▲, ■, and + in Fig. 4). Based on all of the data presented in Fig. 4, Eq. (2) has been proved to be quite accurate (within 1 deg of the corresponding computational or experimental value) for the range $0 \leqq \alpha \leqq 20$ deg and $0 \leqq \lambda \leqq 70$ deg at all Mach numbers examined. Out of this range, the prediction becomes less accurate. It is important to note that this procedure is not applicable for the range where α is above the theoretical attachment limit for the two-dimensional oblique shock at a certain M because β_{os} is not obtainable for Eq. (2) under such a condition.

In terms in Eq. (2), β can be easily specified for arbitrary M, α, and λ within the effective range of Eq. (2). As long as the shock remains attached to the wing apex, the trace of the shock in the plane of symmetry is a straight line. Hence the inviscid strake-shock location can be specified on the wall using Eq. (2).

Conclusions

Parametric calculations of supersonic flowfields around a series of rhombic delta wings were carried out to construct a correlation law for predicting the shock angle in the plane of symmetry of the wing. The computed shock angles were correlated by a parameter comprising Mach number, the theoretical two-dimensional oblique shock angle, and the angle between the plane of symmetry and the face of the rhombic wing. By approximating the correlated data using a polynomial fit, a correlation law of the shock angle with supersonic Mach number and wing geometry has been constructed.

References

[1]Koide, S., "The Effects of Junction Modifications on Sharp-Fin-Induced Glancing Shock Wave/Boundary Layer Interaction," Ph.D. Thesis, Cranfield Univ., Bedford, England, UK, June 1994; see also Koide, S., and Stollery, J. L., "Effects of Junction Modifications on Sharp-Fin-Induced Shock Wave/Boundary Layer Interaction," AIAA Paper 93-2935, July 1993.

[2]Koide, S., Griesel, C. J. W., and Stollery, J. L., "Effects of Strakes on a Glancing Shock Wave/Turbulent Boundary Layer Interaction," *Journal of Aircraft*, Vol. 32, No. 5, 1995, pp. 985–992.

[3]Griesel, C. J. W., "Space Marching with Rieman-Solver Adaptations Applied to Three Dimensional Flows," M.S. Thesis, Cranfield Univ., Bedford, England, UK, March 1993.

[4]Deng, X., Liao, J., and Zhang, H., "Improvement of Conical Similarity Rules in Swept Shock Wave/Boundary Layer Interaction," AIAA Paper 93-2941, July 1993.

[5]Liao, J., and Deng, X., "A Simple Similarity Law of Conical Shock Wave," AIAA Paper 94-2308, June 1994.

Eigenvector Derivatives for Doubly Repeated Eigenvalues

Ting-Yu Chen*
National Chung Hsing University, Taichung, Taiwan 40227, Republic of China

Introduction

THE calculation of eigenvector derivatives with respect to a design variable has been discussed by various researchers.[1–3] If the eigensystem has distinct eigenvalues, these methods compute the eigenvector derivatives analytically. If, however, repeated eigenvalues occur in the system, the eigenvector derivatives with repeated eigenvalues can not be obtained by these methods. Ojalvo,[4] Dailey,[5] and Mills-Curran[6,7] addressed this problem and developed some approaches to compute the eigenvector derivatives.

Mills-Curran's method[6,7] was proved to be the most general one in solving this problem. In his approach the eigenvector derivatives with repeated eigenvalues are assumed to be equal to an unknown vector plus a linear combination of the eigenvectors with repeated eigenvalues. The unknown vector is determined by solving a set of linear equations. The coefficient matrix of these linear equations is obtained by deleting some rows and columns of the original singular eigenmatrix. A procedure was provided in his paper to find the nonsingular submatrix from the singular eigenmatrix with a higher order deficiency. For complex structures the procedure may become tedious.

It is found in this research that for a special case there is no need to employ Mills-Curran's method to compute the eigenvector derivatives with repeated eigenvalues. The eigenvector derivatives with repeated eigenvalues can still be computed using Fox and Kapoor's approach.[1] The special case is defined as follows. The design variable change affects the stiffness in only one direction and the mass matrix is not affected. If the system has identical stiffness in two directions, then the occurrence of doubly repeated eigenvalues can be expected. Owing to the dynamic characteristics of the structure, one of the eigenvalue sensitivities for the doubly repeated eigenvalues is zero.

Many structures have these characteristics.[8] For example, a cantilever beam has identical moments of inertia in the y and z directions. The occurrence of repeated eigenvalues is expected due to the existence of two identical perpendicular bending modes. If the change of any of the moments of inertia does not affect the other moment of inertia and the mass matrix, then the structure fulfills the definition of the problem.

Theoretical Derivation

Let

$$[F_i] = [K] - \lambda_i[M]; \qquad i = 1, 2 \tag{1}$$

where $[K]$ is the stiffness matrix, $[M]$ the mass matrix, and λ_i the repeated eigenvalue.

The eigenproblem is expressed as

$$[F_i]\{\phi_i\} = 0; \qquad i = 1, 2 \tag{2}$$

where $\{\phi_i\}$ are the orthonormal eigenvectors associated with the repeated eigenvalue.

It is well known that the eigenvectors associated with the repeated eigenvalues are not unique. They can be the linear combination of the eigenvectors associated with the repeated eigenvalues,

$$\{\bar{\phi}_i\} = [\Phi]\{a_i\}; \qquad i = 1, 2 \tag{3}$$

where $[\Phi]$ contains the two eigenvectors associated with the repeated eigenvalues. In Eq. (3), $\{\bar{\phi}_i\}$ is the eigenvector based on a specific linear combination.

The weighting coefficients in $\{a_i\}$ can be obtained by solving the following subeigenproblem:

$$\left([\Phi]^T([K]' - \lambda_i[M]')[\Phi] - \lambda_i'[I]\right)\{a_i\} = 0; \qquad i = 1, 2 \tag{4}$$

where $[K]'$ and $[M]'$ are the derivatives of the stiffness and the mass matrices with respect to the design variable, respectively; λ_i' is the eigenvalue derivative that is also the eigenvalue of the subeigenproblem; and $[I]$ is the unit matrix.

If the eigenvalues of this subeigenproblem are distinct, then the eigenvectors of the original system are uniquely determined by Eq. (3). The eigenproblem (2) now becomes

$$[F_i]\{\bar{\phi}_i\} = 0; \qquad i = 1, 2 \tag{5}$$

Taking the derivatives of Eq. (5) with respect to a design variable yields

$$[F_i]\{\bar{\phi}_i\}' = -[F_i]'\{\bar{\phi}_i\}; \qquad i = 1, 2 \tag{6}$$

where $\{\bar{\phi}_i\}'$ and $[F_i]'$ are the derivatives of $\{\bar{\phi}_i\}$ and $[F_i]$, respectively.

Assume

$$\{\bar{\phi}_i\}' = \sum_{l=1}^{n} c_{li}\{\phi_l\}; \qquad i = 1, 2 \tag{7}$$

where n is the number of the degrees of freedom of the system. Substituting Eq. (7) into Eq. (6) and premultiplying Eq. (6) by $\{\phi_j\}^T$ gives

$$\{\phi_j\}^T[F_i]c_{ji}\{\phi_j\} = -\{\phi_j\}^T[F_i]'\{\bar{\phi}_i\} \tag{8}$$

or

$$c_{ji}(\lambda_j - \lambda_i) = -\{\phi_j\}^T[F_i]'\{\bar{\phi}_i\} \tag{9}$$

or

$$c_{ji} = -\frac{\{\phi_j\}^T[F_i]'\{\bar{\phi}_i\}}{\lambda_j - \lambda_i} \tag{10}$$

Received July 14, 1993; revision received Aug. 1, 1995; accepted for publication Aug. 1, 1995.

*Professor, Department of Mechanical Engineering.